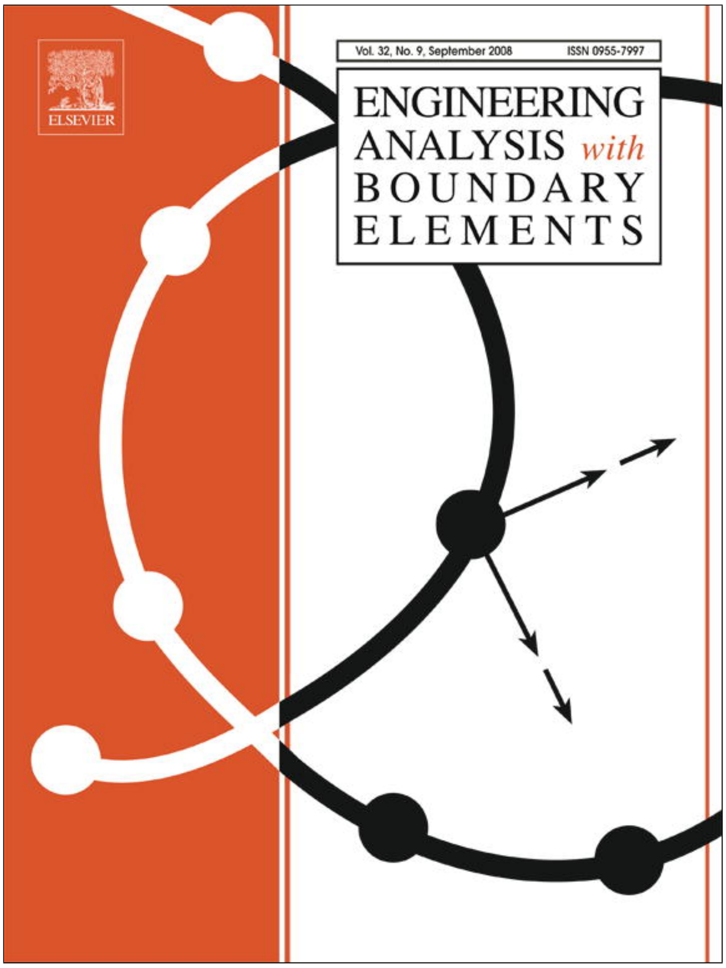
Vol. 32, No. 9, September 2008
ISSN 0955-7997
ENGINEERING
ANALYSIS with
BOUNDARY
ELEMENTS
ELSEVIER

ELSEVIER

Engineering Analysis with Boundary Elements 32 (2008) 704–712

ENGINEERING ANALYSIS with BOUNDARY ELEMENTS

www.elsevier.com/locate/enganabound

Meshless approach for thermo-mechanical analysis of functionally graded materials

Hui Wang[a], Qing-Hua Qin[b,*]

[a]*College of Civil Engineering and Architecture, Henan University of Technology, Zhengzhou 450052, PR China*
[b]*Department of Engineering, Australian National University, Canberra, ACT 0200, Australia*

Received 23 August 2007; accepted 8 November 2007
Available online 21 February 2008

Abstract

On the basis of analog equation theory, the method of fundamental solutions coupling with radial basis functions (MFS–RBF), a meshless algorithm is developed to simulate the static thermal stress distribution in two-dimensional (2D) functionally graded materials (FGMs). The analog equation method (AEM) is used to obtain the equivalent homogeneous system to the original nonhomogeneous equation, after which RBF and MFS are used to construct the related approximated particular part and complementary part, respectively. Finally, all unknowns are determined by satisfying the governing equations in terms of displacement components and boundary conditions. Numerical experiments are performed for different 2D structures made of FGMs, and the proposed meshless method is validated by comparing available analytical and numerical results.

Keywords: Meshless method; Analog equation method; Method of fundamental solutions; Radial basis functions; Functionally graded materials

1. Introduction

Functionally graded materials (FGMs) have been attracting attention due to their continuously and smoothly varying material properties, which distinguish FGMs from laminated composite materials, in which the abrupt change in material properties across the interface between layers can result in large interlaminar stresses leading to delamination. FGMs can be made to utilize the desirable properties of their individual constituents, allowing for spatial optimization by grading the volume fractions of two or more constituents to improve the response of structures. For instance, a smooth transition between a pure metal and a pure ceramic may result in a multifunctional material that combines the desirable high temperature properties and thermal resistance of the ceramic with the fracture toughness and strength of the metal.

Generally speaking, FGMs can be viewed as special inhomogeneous materials whose properties are dependent on spatial coordinates. So far, two models have been used to characterize the material gradation. One is the continuum model in which analytical functions such as exponent and power-law functions are commonly used to describe the continuously varying material properties. Although the continuum model may not be physical in practice, this model is convenient for conducting mathematical analysis. The other is the micromechanics model, which takes into account the interactions between the constituent phases and uses a certain representative volume element (RVE) to estimate the average local stress and strain fields of the composite, after which the local average fields are used to evaluate the efficient material properties. The Mori–Tanaka method and the self-consistent method are two representatives of these models [1,2]. In this paper, attention is focused on the continuum model only.

Although analytical approaches can provide closed-form solutions, they are limited to simple geometries, certain types of gradation of material properties, specific types of boundary conditions and special loading cases. To perform more general analysis, we need to resort to various numerical methods.

In recent years, as alternatives to the classic finite element method (FEM) and boundary element method

*Corresponding author.
E-mail address: qinghua.qin@anu.edu.au (Q.-H. Qin).

0955-7997/$ - see front matter
doi:10.1016/j.enganabound.2007.11.001

(BEM), meshless methods have been used which employ a set of scattered points instead of elements to approximate solutions, exhibiting the advantages of avoiding mesh generation, simple data preparation, easy post-processing and so on. The corresponding developments in thermal and stress computation in FGMs include: Rao and Rahman [3] used element-free Galerkin method (EFGM) to simulate stress fields near the crack tip in FGMs. The same method was used by Dai et al. [4] to study thermo-mechanical behavior of FGM plates. Ching and Yen [5,6] analyzed the static and transient responses of FGMs under mechanical and thermal loads by means of the meshless local Petrov–Galerkin (MLPG) method, which was also used to perform stress analysis in anisotropic FGMs [7]. Moreover, Sladek et al. [8] solved dynamic anti-plane shear crack problem in FGMs by a meshless local boundary integral equation (LBIE) method. They also used the same method to analyze the transient heat conduction in anisotropic and functionally graded media [9]. Qian et al. [10] studied the static and dynamic deformations of thick functionally graded elastic plates with higher-order plate theory by means of MLPG method.

The objective of the paper is to develop a meshless algorithm, based on AEM, MFS [11], and RBF, for analyzing two-dimensional (2D) thermo-mechanical problems in FGMs. It is well known that most MFS-based meshless numerical methods, such as the virtual boundary collocation method [12,13], the F-Trefftz method [14], the charge simulation method [15] and the singularity method [16], are efficient in solving certain homogeneous problems. When dealing with nonzero body forces or complex problems in which the corresponding fundamental solutions are difficult to be obtained, the abovementioned methods seem very inefficient. To overcome this difficulty, an efficient meshless numerical algorithm is proposed by combining use of radial basis functions (RBF) [17,18], AEM [19], and MFS. In the algorithm, the analog equation method (AEM) is used to obtain the equivalent homogeneous system to the original nonhomogeneous equation, and then RBF and MFS are used to approximate the related particular part and complementary part, respectively. Finally, all unknowns are determined by enforcing satisfaction of the governing equations at interpolation points and boundary conditions at boundary nodes. The approach proposed in Refs. [20,21] is used to conduct steady-state and transient thermal analysis of FGMs and other inhomogeneous material with the proposed meshless method.

The paper is organized as follows: Section 2 provides a full description of the 2D thermo-mechanical system in FGMs. In Section 3, the detailed solution procedure is presented. Numerical results are demonstrated and discussed in Section 4 and conclusions are presented in Section 5.

2. Statement of thermo-mechanical systems in FGMs

In this section, the basic formulations of thermo-elasticity in FGMs are reviewed, so that the paper is self-contained. For convenience of presentation, the Cartesian tensor notation is adopted. The comma in the following equations indicates a space derivative, and the same subscript appearing twice in an equation represents summation. Because FGMs can be viewed without loss of generality as isotropic nonhomogeneous materials, the following formulations and processes are provided for general thermo-mechanics problems in general 2D elastic solids.

2.1. Governing equations

Let us consider an isotropic and linear elastic domain Ω bounded by the boundary Γ. The Cartesian coordinates $\mathbf{x}=\{x_1,x_2\}^{\mathrm{T}}$ are used to describe infinitesimal static deformations. Static equilibrium requires

$$\sigma_{ij,j}+b_i=0 \quad \text{in } \Omega, \tag{1}$$

where σ_{ij} denotes the components of Cauchy stress tensor and b_i the components of body force per unit volume.

For an isotropic elastic material, the constitutive equation related to stresses and strains is stated in the form

$$\sigma_{ij}=\tilde{\lambda}\delta_{ij}\varepsilon_{kk}+2\tilde{\mu}\varepsilon_{ij}-\tilde{m}\delta_{ij}T, \tag{2}$$

where $\tilde{\lambda}=(2\tilde{v}/(1-2\tilde{v}))\tilde{\mu}$, $\tilde{\mu}=(E/2(1+v))$, $\tilde{m}=(\tilde{\alpha}\tilde{E}/(1-2\tilde{v}))$. $\tilde{E},\tilde{v},\tilde{\alpha}$ have different values for plane stress and plane strain states such as

$$\begin{cases} \tilde{E}=E & \tilde{v}=v & \tilde{\alpha}=\alpha & \text{for plane strain,} \\ \tilde{E}=\dfrac{1+2v}{(1+v)^2}E & \tilde{v}=\dfrac{v}{1+v} & \tilde{\alpha}=\dfrac{1+v}{1+2v}\alpha & \text{for plane stress,} \end{cases}$$

and parameters $E(\mathbf{x})$, $v(\mathbf{x})$ and $\alpha(\mathbf{x})$ are functions of space coordinates $\mathbf{x}$ and represent elastic modulus, Poisson ratio, and linear coefficient of thermal expansion, respectively. T denotes the temperature change the material experiences, that is, the final temperature minus the original temperature. If the change in temperature is positive we have thermal expansion, and if negative, thermal contraction.

If the displacements are small enough that the square and product of its derivatives are negligible, then the relation of Cauchy strains and displacements can be written as

$$\varepsilon_{ij}=\frac{1}{2}(u_{i,j}+u_{j,i}). \tag{3}$$

The boundary value problem defined by Eqs. (1)–(3) is completed by adding the following displacement and surface traction boundary conditions:

$$\begin{aligned} &u_i=\bar{u}_i && \text{on } \Gamma_u, \\ &t_i=\sigma_{ij}n_j=\bar{t}_i && \text{on } \Gamma_t, \end{aligned} \tag{4}$$

where $\bar{u}_i$ is the prescribed displacements on Γ_u and $\bar{t}_i$ is the given tractions on Γ_t. Γ_u and Γ_t are complementary parts of the boundary Γ. n_j represents the direction cosines of the unit outward normal to the boundary.

Substituting Eqs. (2) and (3) into Eq. (1) yields the second-order partial differential equation (PDE) in terms

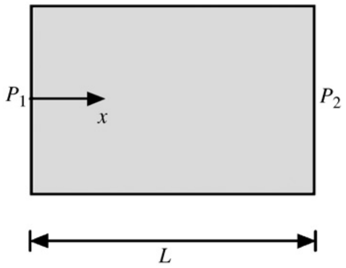

Fig. 1. Demonstration of material properties of FGMs.

Table 1
Classic power-law and exponential distributions of material property in FGM

	Power-law distribution	Exponential distribution
Volume fraction	$V(x) = (x/L)^{\eta}$	$V(x) = e^{\eta(x/L)}$
Material property	$P(x) = (1-V(x))P_1 + V(x)P_2$	$P(x) = V(x)P_1$

of displacement components

$$(\tilde{\lambda} + \tilde{\mu})u_{k,ki} + \tilde{\mu}u_{i,kk} + \tilde{\lambda}_{,i}u_{k,k} + \tilde{\mu}_{,k}(u_{i,k} + u_{k,i}) - \tilde{m}T_{,i} - \tilde{m}_{,i}T + b_i = 0. \tag{5}$$

2.2. Graded types of FGM

Material properties of FGMs are usually defined by the variation in the volume fractions. In the literature, there two common descriptions to the variation of volume fractions: the power-law assumption and exponential assumption [22,23]. In order to clearly show the variation of material properties with different assumptions, for example, we consider the material shown in Fig. 1 graded through the length L along the x direction. If the material properties of two constituents are P_1 and P_2, respectively, then the general material property P of the FGM is given in Table 1 for two different distributions.

3. Solution procedure

3.1. Analog equation method (AEM)

For the thermo-elastic Eq. (5) describing displacement responses in general nonhomogeneous media, the fundamental solutions are difficult to obtain in a closed form. However, we can circumvent this obstacle by indirect ways. From the viewpoint of mathematics, the displacement fields must be in terms of space coordinates, regardless of the particular forms of elastic properties and loading types. So, we can design an equivalent elastic system written as

$$(\widehat{\lambda} + \widehat{\mu})u_{k,ki} + \widehat{\mu}\,u_{i,kk} + \widehat{b}_i = 0 \tag{6}$$

to replace Eq. (5), where $\widehat{\lambda}, \widehat{\mu}$ are elastic constants of a fictitious isotropic homogeneous solid and $\widehat{b}_i$ the 'body force' induced by the displacement distributions sought and the temperature distribution.

In the following, we derive the general solutions of Eq. (6) by means of RBF approximation and MFS in the new equivalent system.

The advantage of MFS based on the superposition of fundamental solutions is that it can conveniently treat homogeneous problems. To determine the particular solutions related to fictitious body forces, RBF approximation is employed in the paper. Based on this idea, we first divide the displacements into two parts:

$$u_i = u_i^h + u_i^p, \tag{7}$$

where the particular parts u_i^p satisfy

$$(\widehat{\lambda} + \widehat{\mu})u_{k,ki}^p + \widehat{\mu}\,u_{i,kk}^p + \widehat{b}_i = 0 \tag{8}$$

in the infinite domain, while the complementary parts, that is, the homogeneous parts, satisfy

$$(\widehat{\lambda} + \widehat{\mu})u_{k,ki}^h + \widehat{\mu}\,u_{i,kk}^h = 0. \tag{9}$$

Obviously, the particular solutions and homogeneous solutions satisfying Eqs. (8) and (9), respectively are not unique, without considering the constraints of boundary conditions.

Next, we use MFS and RBF to obtain the two parts discussed above.

3.2. Radial basis functions (RBF) approximation

RBF are usually expressed in terms of Euclidian distance, so they can work well in any dimensional space and do not increase computational cost. Due to these advantages, RBFs have been widely used in many aspects over the past 10 years. In this section, RBFs are used to derive the displacement particular solutions.

Firstly, the body forces in Eq. (8) are approximated by

$$\widehat{b}_i(\mathbf{x}) = \sum_{m=1}^{M} \phi^m(\mathbf{x})\alpha_i^m = \sum_{m=1}^{M} \delta_{li}\phi^m(\mathbf{x})\alpha_l^m, \tag{10}$$

where M is the number of interpolating points in the domain, α_i^m are coefficients to be determined, and ϕ^m is a set of RBFs.

Similarly, the particular solution u_i^p is also approximated by means of the same coefficient set

$$u_i^p(\mathbf{x}) = \sum_{m=1}^{M} \Phi_{li}^m(\mathbf{x})\alpha_l^m, \tag{11}$$

where Φ_{li}^m is a corresponding set of approximate particular solutions. Because the particular solution u_i^p satisfies Eq. (8), the precondition to this process is that such relations as

$$(\widehat{\lambda} + \widehat{\mu})\Phi_{lk,ki}^m(\mathbf{x}) + \widehat{\mu}\,\Phi_{li,kk}^m(\mathbf{x}) = -\delta_{li}\phi^m(\mathbf{x}) \tag{12}$$

hold.

For the piecewise smooth power spline (PS), also known as conical spline, $\phi = r^{2n-1}$, and thin plate spline (TPS), also called Duchon spline, $\phi = r^{2n}\ln r$, the corresponding set of particular solutions and its first and second order differentials, respectively, are given in the Appendix for plane strain states [18].

3.3. Method of fundamental solutions (MFS)

To obtain approximated solutions of homogeneous Eq. (9), N fictitious source points $\mathbf{y}_n$ $(n = 1,2,\ldots,N)$ located on the virtual boundary outside the domain are selected (Fig. 2). Moreover, assume that at each source point there is a pair of fictitious point loads φ_1^i, φ_2^i along x and y direction, respectively. According to the main construct of MFS, the approximated displacement fields at arbitrary points $\mathbf{x}$ in the domain or on the boundary can be expressed as a linear combination of fundamental solutions in terms of fictitious sources outside the domain of interest, that is,

$$u_i^h(\mathbf{x}) = \sum_{n=1}^{N} u_{li}^*(\mathbf{x}, \mathbf{y}_n)\varphi_l^n \tag{13}$$

in which the displacement fundamental solution $u_{li}^*(\mathbf{x}, \mathbf{y})$ denoting the induced displacement distribution along the i direction at the field point $\mathbf{x}$ due to the unit concentrated load acting in the l direction at source point $\mathbf{y}$ satisfies the Navier equation

$$(\widehat{\lambda} + \widehat{\mu})u_{lk,ki}^*(\mathbf{x}, \mathbf{y}) + \widehat{\mu}\, u_{li,kk}^*(\mathbf{x}, \mathbf{y}) = -\delta_{xy}e_{li} \tag{14}$$

such that δ is the Dirac delta function concentrated at the source point $\mathbf{y}$ and e_{li} are the components of the 2×2 identity matrix.

It is apparent that Eq. (13) completely satisfies Eq. (9) in the domain based on the definition of the fundamental solutions, that is Eq. (14), and the fact that source point $\mathbf{y}_n$ and field point $\mathbf{x}$ are different.

The related expressions of fundamental solutions and the derivatives for the plane strain state can be found in Appendix.

3.4. Final complete solutions

According to Eq. (7), the complete solutions of displacement components are written as the sum of the particular and homogeneous solutions, thus

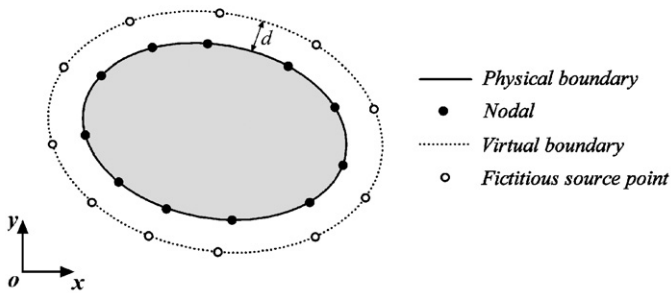

Fig. 2. Virtual and physical boundary of arbitrary domain.

$$u_i(\mathbf{x}) = \sum_{n=1}^{N} u_{li}^*(\mathbf{x}, \mathbf{y}_n)\varphi_l^n + \sum_{m=1}^{M} \Phi_{li}^m(\mathbf{x})\alpha_l^m. \tag{15}$$

Differentiating Eq. (15) yields

$$u_{i,j}(\mathbf{x}) = \sum_{n=1}^{N} u_{li,j}^*(\mathbf{x}, \mathbf{y}_n)\varphi_l^n + \sum_{m=1}^{M} \alpha_l^m \Phi_{li,j}^m(\mathbf{x}), \tag{16}$$

$$u_{i,jk}(x) = \sum_{n=1}^{N} u_{li,jk}^*(\mathbf{x}, \mathbf{y}_n)\varphi_l^n + \sum_{m=1}^{M} \alpha_l^m \Phi_{li,jk}^m(\mathbf{x}). \tag{17}$$

Consequently, the stress components can be expressed by substituting Eqs. (16) and (17) in Eqs. (2) and (3) as

$$\sigma_{ij}(\mathbf{x}) = \sum_{n=1}^{N} \sigma_{lij}^*(\mathbf{x}, \mathbf{y}_n)\varphi_l^n + \sum_{m=1}^{M} S_{lij}^m(\mathbf{x})\alpha_l^m - \tilde{m}\delta_{ij}T, \tag{18}$$

where

$$\sigma_{lij}^* = \tilde{\lambda}\delta_{ij}u_{lk,k}^* + \tilde{\mu}(u_{li,j}^* + u_{lj,i}^*),$$
$$S_{lij}^m = \tilde{\lambda}\delta_{ij}\Phi_{lk,k}^m + \tilde{\mu}(\Phi_{li,j}^m + \Phi_{lj,i}^m). \tag{19}$$

Furthermore, the traction components can be derived as

$$t_i = \sigma_{ij}n_j = \sum_{n=1}^{N} t_{li}^*\varphi_l^n + \sum_{m=1}^{M} P_{li}^m\alpha_l^m - \tilde{m}n_iT, \tag{20}$$

where $t_{li}^* = \sigma_{lij}^* n_j$ and $P_{li}^m = S_{lij}^m n_j$.

Finally, making Eqs. (16) and (17) satisfy the governing Eq. (5) at M interpolation points and substituting Eqs. (15) and (20) into boundary conditions (Eq. (4)) at N boundary nodes produce a set of linear algebraic equations in matrix form for the determination of unknown coefficients

$$[\mathbf{H}]\{\mathbf{A}\} = \{\mathbf{B}\}, \tag{21}$$

where vector $\{\mathbf{A}\} = \{\varphi_1^1 \quad \varphi_2^1 \quad \cdots \quad \cdots \quad \varphi_1^N \quad \varphi_2^N \quad \alpha_1^1 \quad \alpha_2^1 \quad \ldots \quad \ldots \alpha_1^M \quad \alpha_2^M\}^{\mathrm{T}}$.

The first and second order derivatives of kernel functions u_{li}^* and Φ_{li}^m used in above process are given in Appendix.

For simplicity, the temperature distribution used in the following computation is taken in an analytical form, rather than numerical solution obtained from a boundary value problem of heat conduction. It should be, however, mentioned that the idea of MFS with RBF also can be used to obtain the numerical distribution of temperature in FGM and the detailed procedure has been documented in Refs. [20,21].

4. Numerical assessment

In this section, three examples of FGM subjected to mechanical or thermal loads are considered to assess the proposed algorithm. In all three examples, except for Poisson's ratio, the material properties vary exponentially or according to a power law. This is a reasonable assumption, since variation on the Poisson's ratio is usually small compared with that of other properties. Finally, to assess the accuracy and convergence of the approximation, the average relative error $Arerr(\zeta)$

defined by

$$Arerr(\zeta) = \sqrt{\frac{\sum_{j=1}^{L}(\zeta_j - \tilde{\zeta}_j)^2}{\sum_{j=1}^{L}(\zeta_j)^2}} \tag{22}$$

is introduced, where ζ_j and $\tilde{\zeta}_j$ are, respectively, the analytical and numerical results of variable ζ at the points of interest, and L is the total number of these points.

Additionally, in the practical computation, the source points $\mathbf{y}_s$ outside the domain are generated by [12,24]

$$\mathbf{y}_s = \mathbf{x}_b + \gamma(\mathbf{x}_b - \mathbf{x}_c) \tag{23}$$

in which $\mathbf{x}_b$ is a boundary node, $\mathbf{x}_c$ is the geometric center of the domain and γ is a dimensionless parameter, which is chosen as 1.0 for outer boundary and -0.5 for inner boundary in our work.

4.1. Hollow circular plate under radial internal pressure

Consider a hollow circular plate as shown in Fig. 3 with inner radius $a = 5$ mm and outer radius $b = 10$ mm under internal radial pressure. Suppose the plate is graded along the radial direction so that elastic modulus $E(r) = E_0(r/a)^\eta$. For $\eta > 0$, the Young's modulus increases as the radius r increases. As $\eta = 0$, the problem is reduced to the analysis of homogeneous media. Analytical solutions of stress components [25] for the case of plane stress state are given in closed form

$$\sigma_r = -\frac{a^{-(\eta/2)}r^{-1-(k/2)+(\eta/2)}}{b^k - a^k}a^{1+(k/2)}(b^k - r^k)p_a,$$
$$\sigma_\theta = \frac{a^{-(\eta/2)}r^{-1-(k/2)+(\eta/2)}}{b^k - a^k} \times \left[\frac{(2+k\nu-\eta\nu)r^k}{k-\eta+2\nu} - \frac{(-2+k\nu+\eta\nu)b^k}{k+\eta-2\nu}\right]a^{1+(k/2)}p_a, \tag{24}$$

with $k = \sqrt{\eta^2 + 4 - 4\eta\nu}$.

In the practical computation, Poisson's ratio, and elastic modulus at the internal surface as well as internal pressure, respectively, are assumed to be $\nu = 0.3$, $E(a) = 200$ GPa, $p_a = 50$ MPa. Figs. 4 and 5 display the convergent performance of the proposed meshless method when the PS basis function r^3 is used. It is found from Figs. 4 and 5 that the accuracy increases with an increase in M or N.

In order to investigate the variation of radial and hoop stresses along the radial direction for various graded parameters η, 32 boundary nodes and 140 interior interpolation points are used. Comparisons between analytical solutions and numerical results are shown in Fig. 6. It is found that regardless of the value of η, radial stress increases monotonously from the inner to the outer surface, whereas hoop stress does not. As η increases, the value of radial stress decreases at any point in the cylinder, except for the points on the boundary, whereas the maximum hoop stress occurs on the inner surface when $\eta = 0$ and on the outer surface when $\eta = 3$. The variation in the hoop stress looks like rotation around a center when η increases. It is also found that the variation in hoop stress

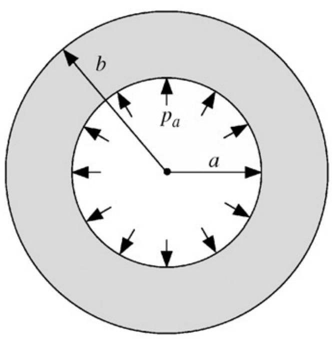

Fig. 3. Configuration of hollow circular plate under internal pressure.

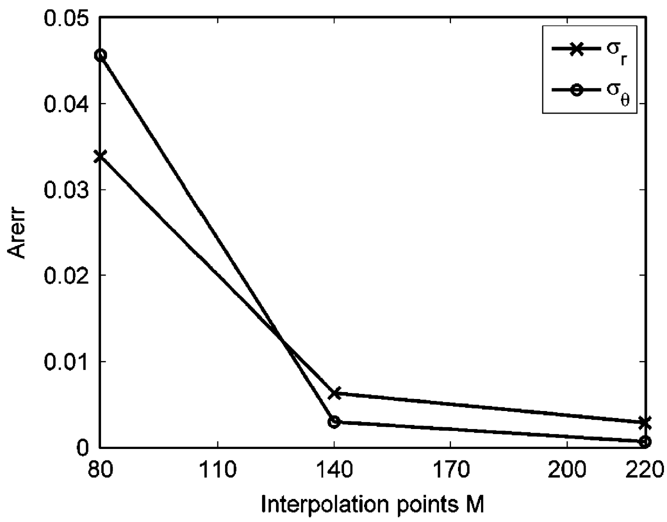

Fig. 4. Convergent performance vs M ($\eta = 2$, $N = 32$).

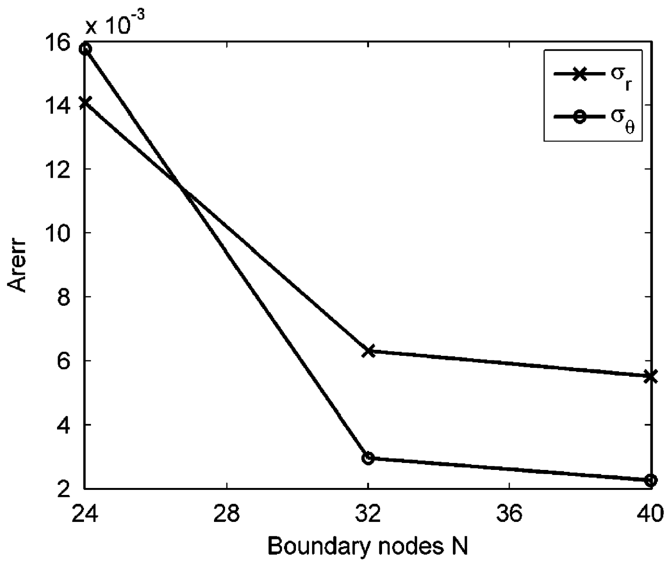

Fig. 5. Convergent performance vs N ($\eta = 2$, $M = 140$).

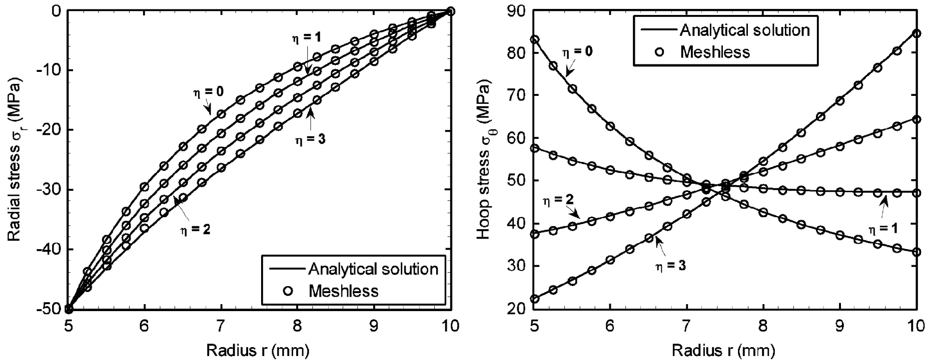

Fig. 6. Distribution of radial and hoop stresses with various graded parameter when 32 boundary nodes and 140 interior interpolation points are used.

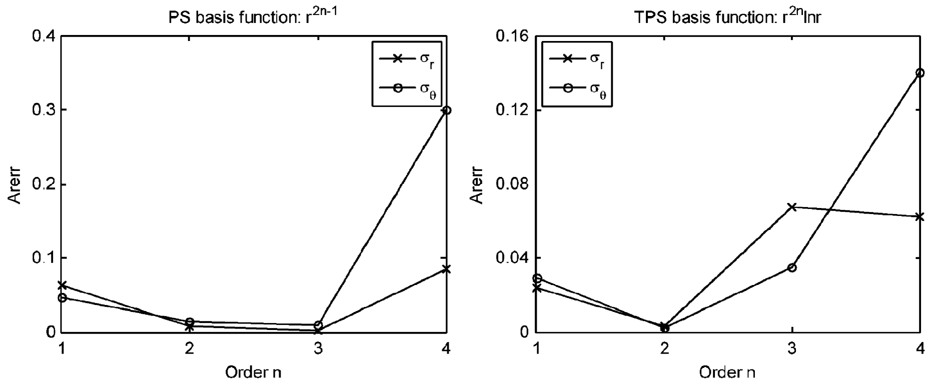

Fig. 7. Effect of orders of radial basis functions when 32 boundary nodes and 220 interior interpolation points are used for the case of.

in FGMs becomes worse when η increases. Therefore, to avoid material instability, the graded parameter should be smaller than specific values.

In this example, the effects of the types and orders of RBF are also tested for the case of the high graded parameter $\eta = 4$. Fig. 7 shows the average relative error distributions. It is evident that a higher order of RBF does not always result in better accuracy. The calculation indicates that r^3 and r^5 in PS, and $r^2 \ln r$ and $r^4 \ln r$ in TPS seem to be able to produce relatively high accuracy in this example. Moreover, TPS has better accuracy than PS. Therefore, $r^4 \ln r$ is used in the remaining computation.

4.2. Functionally graded elastic beam under sinusoidal transverse load

An elastic beam as shown in Fig. 8 is considered in this example, which is made of two-phase Al/SiC composite. The elastic modulus varying exponentially in the z direction is given by $E(z) = E_0 e^{\eta z}$. The left and right end faces of the FG beam are assumed to be simply supported such that

$$w(0,z) = w(L,z) = 0,$$
$$t_x(0,z) = t_x(L,z) = 0. \tag{25}$$

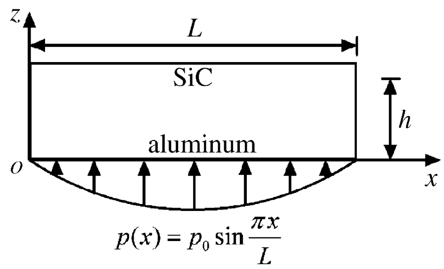

Fig. 8. Functionally graded beam subjected to symmetric sinusoidal transverse loading.

The top surface of the beam is assumed to be free of mechanical force and the bottom surface is subjected to a distributed load p as shown in Fig. 8:

$$t_x(x,0) = t_x(x,h) = 0,$$
$$t_z(x,0) = p,\, t_z(x,h) = 0. \tag{26}$$

The problem is solved under a plane strain assumption with the length $L = 100\,\text{mm}$ and thickness $h = 40\,\text{mm}$. The material properties of aluminum and SiC are, respectively, $E_{Al} = 70\,\text{GPa}$ and $E_{SiC} = 427\,\text{Gpa}$ $(\eta = (\ln(E_{SiC}/E_{Al})/h))$. The maximum transverse load p_0 is equal to 10 MPa. Total 34 boundary nodes and 169 interior interpolation points are selected in the analysis.

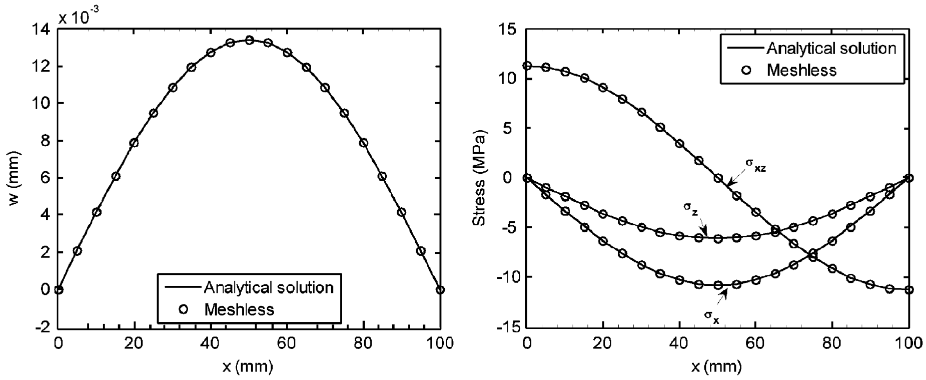

Fig. 9. Transverse displacement and stress components along the line $z = h/2$.

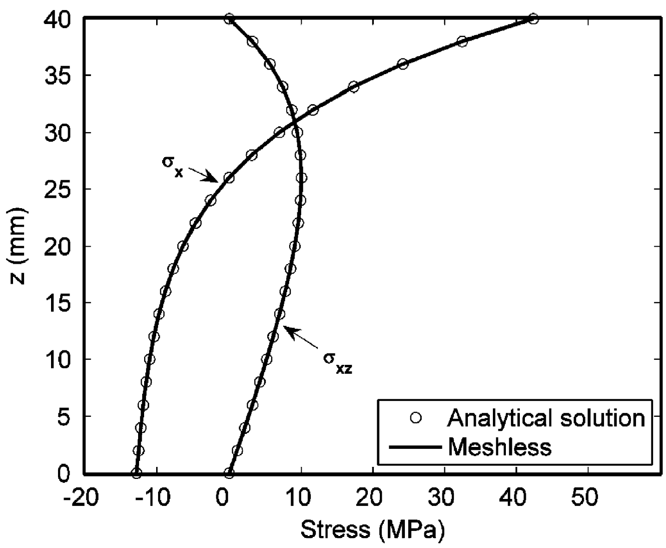

Fig. 10. Variation of stress components along the cross section $x = L/5$.

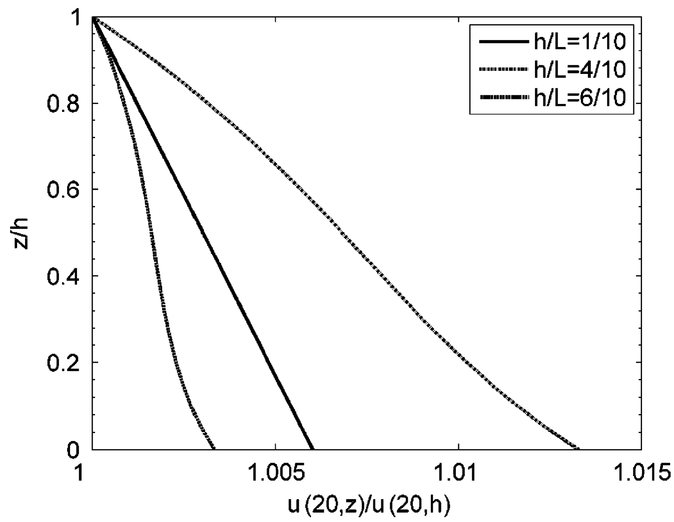

Fig. 11. Shape of transverse cross section after deformation with various ratios of thickness and length.

Figs. 9 and 10 respectively show the variation of transverse displacement and stress components along the line $z=h/2$ and $x=L/5$. Good agreement can be observed between the numerical results and exact solutions [26]. Furthermore, the shapes of cross-sections after deformation are provided in Fig. 11, from which it can be seen that for smaller ratios of thickness and length, for example, $h/L = 1/10$, the cross section approximately maintains plane after deformation. This phenomenon demonstrates the validity of the cross-section assumption in classic thin beam bending theory.

4.3. Symmetrical thermo-elastic problem in a long cylinder

Consider a thick hollow cylinder with same geometries and mechanical boundary conditions as in Fig. 3. The same power-law assumptions are used to define the elastic modulus and coefficient of thermal expansion, that is, $E(r) = E_0(r/a)^\eta$ and $\alpha(r) = \alpha_0(r/a)^\eta$. The temperature change in the entire domain is given in a closed form

$$T = \begin{cases} \dfrac{T_a(b^{-\eta} - r^{-\eta}) + T_b(r^{-\eta} - a^{-\eta})}{b^{-\eta} - a^{-\eta}} & \text{for } \eta \neq 0, \\ \dfrac{T_a \ln(b/r) + T_b \ln(r/a)}{\ln(b/a)} & \text{for } \eta = 0, \end{cases} \tag{27}$$

with $T_a = T(a)$ and $T_b = T(b)$.

The two-phase aluminum/ceramic FGM is examined here. The metal aluminum constituent is arranged on the inner surface, while the ceramic constituent is on the outer surface. The related material properties are $E_{Al} = 70\,\text{GPa}$, $\alpha_{Al} = 1.2 \times 10^{-6}\,°\text{C}^{-1}$, $E_{ceramic} = 151\,\text{GPa}$, $\alpha_{ceramic} = 2.59 \times 10^{-6}\,°\text{C}^{-1}$. Poisson's ratio is taken to be $\nu = 0.3$. The inner and outer boundary temperature changes, respectively, are $T_a = 10\,°\text{C}$ and $T_b = 0\,°\text{C}$.

Analytical solutions of displacements and stresses for the case of plane strain state are provided by Jabbari et al. [27]. However, it is necessary to point out that there are some important written errors in the work of Jabbari et al. The

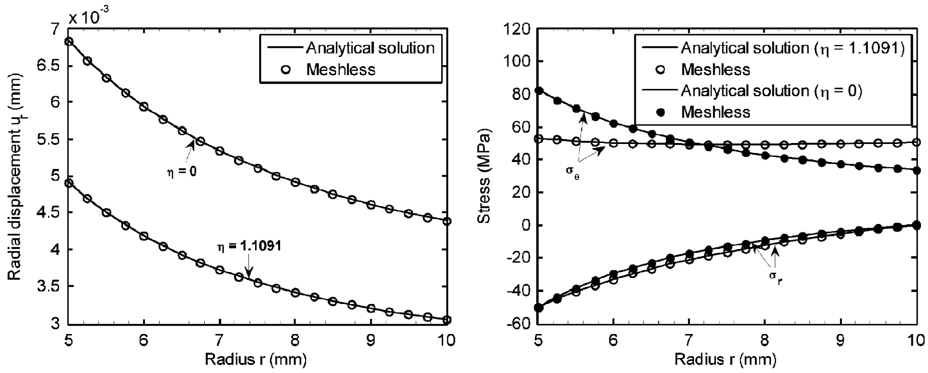

Fig. 12. Stresses and radial displacement distributions in FGM and homogeneous material with $N = 32$, $M = 220$.

results in Fig. 12 show good agreement between the analytical solutions and the numerical results in FGM and homogeneous material, which corresponds to $\eta = 0$. Furthermore, we again find that after graded treatment, the maximum value of hoop stress decreases from 82.6 to 53 MPa. Additionally, the radial displacement in FGM also decreases, compared to the response in homogeneous media. Since the value of radial displacement is very small, radial deformation can be neglected in practical analysis.

5. Conclusions

The paper presents an efficient meshless method for thermo-elastic analysis of FGMs, in which the combination of AEM, MFS and RBF provides a powerful numerical procedure. Numerical experiments show that a good agreement is achieved between the results obtained from the proposed meshless method and available analytical solutions. It is clear that the responses in FGMs differ substantially from those in their homogeneous counterparts. The appropriate graded parameter can lead to low stress concentration and little change in the distribution of stress fields.

Additionally, from the solution procedure in Section 3, we can see that the construction of the full displacement variables is independent of the type of problem considered. This characteristic means that the proposed method can be easily extended to other engineering problems such as multi-phase composites and heterogeneous piezoelectric materials, in addition to FGMs.

Appendix A. First and second order differentials of fundamental solutions and approximated particular solutions

A1. Fundamental solutions and their derivatives

$$u^*_{li} = \frac{1}{8\pi\widehat{\mu}(1-\widehat{v})}\left[(3-4\widehat{v})\delta_{li}\ln\frac{1}{r} + r_{,l}r_{,i}\right],$$

$$u^*_{li,j} = \frac{1}{8\pi\widehat{\mu}(1-\widehat{v})}\frac{1}{r}[-(3-4\widehat{v})\delta_{li}r_{,j} + r_{,i}\delta_{lj} + r_{,l}\delta_{ij} - 2r_{,i}r_{,j}r_{,l}],$$

$$u^*_{lk,k} = \frac{1}{4\pi\widehat{\mu}(1-\widehat{v})}\frac{1}{r}[-(1-2\widehat{v})]r_{,l},$$

$$u^*_{lk,ki} = \frac{1}{4\pi\widehat{\mu}(1-\widehat{v})}\frac{1}{r^2}(1-2\widehat{v})\{2r_{,l}r_{,i} - \delta_{li}\},$$

$$u^*_{li,kk} = \frac{1}{4\pi\widehat{\mu}(1-\widehat{v})}\frac{1}{r^2}\{\delta_{li} - 2r_{,i}r_{,l}\}.$$

A2. Approximated particular solutions and their derivatives

A2.1. Power spline (PS) function

$$\Phi_{li} = -\frac{1}{2\widehat{\mu}(1-\widehat{v})}\frac{1}{(2n+1)^2(2n+3)}r^{2n+1}(A_1\delta_{li} + A_2r_{,l}r_{,i}),$$

$$\Phi_{li,j} = -\frac{1}{2\widehat{\mu}(1-\widehat{v})}\frac{1}{(2n+1)^2(2n+3)}r^{2n}\left[B_1\delta_{li}r_{,j} + B_2(\delta_{lj}r_{,i} + \delta_{ij}r_{,l}) + B_3r_{,i}r_{,j}r_{,l}\right],$$

$$\Phi_{lk,ki} = -\frac{1}{2\widehat{\mu}(1-\widehat{v})}\frac{1}{(2n+1)^2(2n+3)}r^{2n-1}B_4[\delta_{li} + (2n-1)r_{,l}r_{,i}],$$

$$\Phi_{li,kk} = -\frac{1}{2\widehat{\mu}(1-\widehat{v})}\frac{1}{(2n+1)^2(2n+3)}r^{2n-1}(C_1\delta_{li} + C_2r_{,l}r_{,i}),$$

where

$A_1 = (4n+5) - 2\widehat{v}(2n+3)$,

$A_2 = -(2n+1)$,

$B_1 = A_1(2n+1)$,

$B_2 = A_2$,

$B_3 = A_2(2n-1)$,

$B_4 = B_1 + 3B_2 + B_3$,

$C_1 = 2B_2 + B_1(2n+1)$,

$C_2 = 2B_2(2n-1) + B_3(2n+1)$.

A2.2. Thin plate spline (TPS) function

$$\Phi_{li} = -\frac{1}{32\,\widehat{\mu}(1-\widehat{v})}\frac{r^{2n+2}}{(n+1)^3(n+2)^2}(A_1\delta_{il} + A_2 r_{,i} r_{,l}),$$

$$\Phi_{li,j} = -\frac{1}{32\,\widehat{\mu}(1-\widehat{v})}\frac{r^{2n+1}}{(n+1)^3(n+2)^2}\big[B_1 r_{,i} r_{,j} r_{,l} + B_2\delta_{il} r_{,j} + B_3(\delta_{ij} r_{,l} + \delta_{lj} r_{,i})\big],$$

$$\Phi_{lk,ki} = -\frac{1}{32\,\widehat{\mu}(1-\widehat{v})}\frac{r^{2n}}{(n+1)^3(n+2)^2}(C_1 r_{,i} r_{,l} + B_4\delta_{li}),$$

$$\Phi_{li,kk} = -\frac{1}{32\,\widehat{\mu}(1-\widehat{v})}\frac{r^{2n}}{(n+1)^3(n+2)^2}(C_2 r_{,l} r_{,i} + C_3\delta_{il}),$$

where

$$A_1 = -(8n^2 + 29n + 27) + 8\,\widehat{v}(n+2)^2 + 2(n+1)(n+2)[4n + 7 - 4\,\widehat{v}(n+2)]\ln r],$$

$$A_2 = 2(n+1)[(2n+3) - 2(n+1)(n+2)\ \ln\ r],$$

$$B_1 = 2nA_2 - 4(n+1)^2(n+2),$$

$$B_2 = 2(n+1)\Big\{A_1 + (n+2)\Big[4n + 7 - 4\,\widehat{v}(n+2)\Big]\Big\},$$

$$B_3 = A_2,$$

$$B_4 = B_1 + B_2 + 3B_3,$$

$$C_1 = 2nB_4 + 8(n+1)^2(n+2)^2(1 - 2\,\widehat{v}),$$

$$C_2 = 2(n+1)B_1 + 4nB_3 - 8(n+1)^3(n+2),$$

$$C_3 = 2(n+1)B_2 + 2B_3 - 4(n+1)^2(n+2) \times\Big[-4n - 7 + 4\,\widehat{v}(n+2)\Big].$$

References

[1] Mori T, Tanaka K. Average stress in matrix and average elastic energy of materials with misfitting inclusions. Acta Metall 1973;21:571–4.

[2] Hill R. A self-consistent mechanics of composite materials. J Mech Phys Solids 1965;13:213–22.

[3] Rao BN, Rahman S. Mesh-free analysis of cracks in isotropic functionally graded materials. Eng Fract Mech 2003;70:1–27.

[4] Dai KY, Liu GR, Han X, Lim KM. Thermomechanical analysis of functionally graded material (FGM) plates using element-free Galerkin method. Comput Struct 2005;83:1487–502.

[5] Ching HK, Yen SC. Meshless local Petrov–Galerkin analysis for 2D functionally graded elastic solids under mechanical and thermal loads. Composites: Part B 2005;36:223–40.

[6] Ching HK, Yen SC. Transient thermoelastic deformations of 2-D functionally graded beams under nonuniformly convective heat supply. Compos Struct 2006;73:381–93.

[7] Sladek J, Sladek V, Zhang Ch. Stress analysis in anisotropic functionally graded materials by the MLPG method. Eng Anal Bound Elem 2005;29:597–609.

[8] Sladek J, Sladek V, Zhang Ch. A meshless local boundary integral equation method for dynamic anti-plane shear crack problem in functionally graded materials. Eng Anal Bound Elem 2005;29:334–42.

[9] Sladek V, Sladek J, Tanaka M, Zhang Ch. Transient heat conduction in anisotropic and functionally graded media by local integral equation. Eng Anal Bound Elem 2005;29:1047–65.

[10] Qian LF, Batra RC, Chen LM. Static and dynamic deformations of thick functionally graded elastic plates by using higher-order shear and normal deformable plate theory and meshless local Petrov–Galerkin method. Composites: Part B 2004;35:685–97.

[11] Kupradze VD, Aleksidze MA. The method of functional equations for the approximate solution of certain boundary value problems. USSR Comput Math Math Phys 1964;4:82–126.

[12] Sun HC, Zhang LZ, Xu Q, Zhang Y. Nonsingularity boundary element methods. Dalian: Dalian University of Technology Press; 1999 (in Chinese).

[13] Sun HC, Yao WA. Virtual boundary element-linear complementary equations for solving the elastic obstacle problems of thin plate. Finite Elem Anal Des 1997;27:153–61.

[14] Karthik B, Palghat AR. A particular solution Trefftz method for non-linear Poisson problems in heat and mass transfer. J Comput Phys 1999;150:239–67.

[15] Katsurada M. Charge simulation method using exterior mapping functions. Jpn J Ind Appl Math 1994;11:47–61.

[16] Nitsche LC, Brenner H. Hydrodynamics of particulate motion in sinusoidal pores via a singularity method. AIChE J 1990;36:1403–19.

[17] Golberg MA, Chen CS, Bowman H. Some recent results and proposals for the use of radial basis functions in the BEM. Eng Anal Bound Elem 1999;23:285–96.

[18] Cheng AHD, Chen CS, Golberg MA, Rashed YF. BEM for thermoelasticity and elasticity with body force—a revisit. Eng Anal Bound Elem 2001;25:377–87.

[19] Katsikadelis JT. The analog equation method—a powerful BEM-based solution technique for solving linear and nonlinear engineering problems. In: Brebbia CA, editor. Boundary element method XVI. Southampton: CLM Publications; 1994. p. 167–82.

[20] Wang H, Qin QH, Kang YL. A new meshless method for steady-state heat conduction problems in anisotropic and inhomogeneous media. Arch Appl Mech 2005;74:563–79.

[21] Wang H, Qin QH, Kang YL. A meshless method for transient heat conduction in functionally graded materials. Comput Mech 2006;38:51–60.

[22] Bao G, Wang L. Multiple cracking in functionally graded ceramic/metal coatings. Int J Solids Struct 1995;32:2853–71.

[23] Delale F, Erdogan F. The crack problem for a nonhomogeneous plane. ASME J Appl Mech 1983;50:609–14.

[24] Young DL, Jane SJ, Fan CM, et al. The method of fundamental solutions for 2D and 3D Stokes problems. J Comput Phys 2006;211:1–8.

[25] Horgan CO. The pressurized hollow cylinder or disk problem for functionally graded isotropic linearly elastic materials. J Elasticity 1999;55:43–59.

[26] Sankar BV. An elasticity solution for functionally graded beams. Compos Sci Technol 2001;61:689–96.

[27] Jabbari M, Sohrabpour S, Eslami MR. Mechanical and thermal stresses in a functionally graded hollow cylinder due to radially symmetric loads. Int J Pres Ves Pip 2002;79:493–7.